
**Liquid Crystals**
Publication details, including instructions for authors and subscription information:
http://www.informaworld.com/smpp/title~content=t713926090

# Structural analysis of the lyotropic polymorphism of four-stranded aggregates of 2'-deoxyguanosine 3'-monophosphate derivatives

Paolo Mariani[a]; Monica M. De Morais[a]; Giovanni Gottarelli[b]; Gian Piero Spada[b]; Hervé Delacroix[c]; Luisa Tondelli[d]
[a] Istituto di Scienze Fisiche, Facoltà di Medicina, Universitè di Ancona, unità di Ancona, Italy [b] Dipartimento di Chimica Organica 'A. Mangini', Università di Bologna, Bologna, ITALY [c] Centre de Génétique Moléculaire, Laboratoire propre du CNRS, Associé à l'Université Pierre et Marie Curie, Gif-sur-Yvette Cedex, France [d] I.Co.C.E.A.-CNR, Ozzano Emilia, Italy

**To cite this Article** Mariani, Paolo , De Morais, Monica M. , Gottarelli, Giovanni , Spada, Gian Piero , Delacroix, Hervé and Tondelli, Luisa(1993) 'Structural analysis of the lyotropic polymorphism of four-stranded aggregates of 2'-deoxyguanosine 3'-monophosphate derivatives', Liquid Crystals, 15: 6, 757 — 778
**To link to this Article: DOI:** 10.1080/02678299308036497
**URL:** http://dx.doi.org/10.1080/02678299308036497

LIQUID CRYSTALS, 1993, VOL. 15, NO. 6, 757–778

# Structural analysis of the lyotropic polymorphism of four-stranded aggregates of 2′-deoxyguanosine 3′-monophosphate derivatives

by PAOLO MARIANI*†, MONICA M. DE MORAIS†, GIOVANNI GOTTARELLI‡, GIAN PIERO SPADA‡, HERVÉ DELACROIX§ and LUISA TONDELLI¶

† Istituto di Scienze Fisiche, Facoltà di Medicina, Università di Ancona, via Ranieri 65, 60131 Ancona and INFM, unità di Ancona, Italy
‡ Dipartimento di Chimica Organica 'A. Mangini', Università di Bologna, via S. Donato 15, 40127 Bologna, Italy
§ Centre de Génétique Moléculaire, Laboratoire propre du CNRS, Associé à l'Université Pierre et Marie Curie, Avenue de la Terrasse, 91198 Gif-sur-Yvette Cedex, France
¶ I.Co.C.E.A.-CNR, via della Chimica 8, 40064 Ozzano Emilia, Italy

(*Received 20 February 1993; accepted 9 July 1993*)



Guanosine derivatives, dissolved in water, can form chromonic cholesteric and hexagonal phases. The common structural unit is a chiral stack of Hoogsteen-bonded guanosine tetramers. Using optical microscopy, circular dichroism and X-ray diffraction techniques, we have analysed the complex columnar polymorphism of two derivatives of 2′-deoxyguanosine—the 3′-monophosphate d(Gp) and the 3′-monophosphate monoisobutyl ester d(Gp)iBu. As a function of water concentration, both compounds exhibit four different columnar phases: in addition to the well-known cholesteric (Ch) and hexagonal (H) phases, a 2-dimensional square (Sq) lattice and a new hexagonal packing have been observed. In such a structure ($H_b$), two columns are packed in the 3m special positions of co-ordinates 1/3, 2/3 and 2/3, 1/3 of the two-dimensional hexagonal unit cell. The unusual phase sequence appears to be related to the presence of strong short range intercolumnar interactions. Moreover, the easing of stacking constraints on increasing dilution seems to induce a tilting of the guanosine residues which form the tetramers.

## 1. Introduction

The peculiar ability of guanosine and some of its derivatives to self-associate into stable structures has been known for a long time (see, for example, [1–4]). It has been suggested that this special feature mediates the pairing in a parallel fashion of the four homologous chromatids during meiosis and the dimerization of the telomeric ends of chromosomes [5–8], and may have a prebiotic significance in the origin of the genetic code [9].

In recent papers [10, 11] the structure of chromonic phases exhibited by aqueous solutions of the dinucleoside phosphate 2′-deoxyguanylyl(3′-5′)-2′-deoxyguanosine d(GpG), has been described; in particular, solutions of the sodium salt of d(GpG) form hexagonal and cholesteric mesophases at low and high water content, respectively. On the basis of X-ray diffraction and optical microscopy experiments [11, 12], it has been

* Author for correspondence.

0267–8292/93 $10·00 

suggested that these liquid crystalline phases are formed by columnar chiral aggregates with negative diamagnetic anisotropy. Each rod appears to be composed of a stacked array of tetrameric disks, formed by four Hoogsteen-bonded guanosine moieties [4, 13], at the typical distance of about 3·4 Å.

Columnar cholesteric and hexagonal phases have also been observed in the case of the nucleotide 2′-deoxyguanosine-5′-monophosphate d(pG), as well as in its 'trimer' d(GpGpG), 'tetramer' d(GpGpGpG) and 'hexamer' d(GpGpGpGpGpG) [14]. Moreover, with the exclusion of d(pG), which does not form detectable particles at the concentrations investigated, discrete four-stranded aggregates have been observed in isotropic solutions by small angle neutron scattering experiments [15]. The overall structure of the four-stranded columnar aggregates appears to be similar in the liquid crystalline phases and in the isotropic solution and is also similar to that of d(GpG) [11, 12, 14–16] (see also [17]).

In order to obtain further information about the self-association properties of guanosine and in particular to analyse the relative importance of steric interactions, we have studied the lyotropic polymorphism of the ammonium salt of 2′-deoxyguanosine-3′-monophosphate d(Gp) and of its isobutyl ester d(Gp)iBu (see chart). For both compounds, our results indicate a complex columnar polymorphism. The structural properties are discussed on the basis of the particular effects which seem to be determined by the esterification of the OH group in the 3′-position in the stabilization of both columnar packing and tetramer stacking.



## 2. Experimental

### 2.1. *Synthesis of 2′-deoxyguanosine 3′-monophosphate monoisobutyl ester, d(Gp)iBu*

The ammonium salt of 2′-deoxyguanosine-3′-monophosphate was of commercial origin (Sigma, 99 per cent purity). The 2′-deoxyguanosine 3′-monophosphate monoisobutyl ester was prepared as follows: 12 ml (2·4 mmol) of a 0·2 M solution of 2-chlorophenyl-*O*,*O*-bis[1-benzotriazolyl]phosphate in dioxan were added dropwise to 1·53 g of 5′-*O*-dimethoxytrityl-$N^2$-diphenylacetyl-2′-deoxyguanosine (2 mmol) dissolved in 1 ml of anhydrous pyridine. The solution was stirred for 15 min at room temperature under the exclusion of moisture. Then 0·28 ml (3 mmol) of freshly distilled isobutyl alcohol were added: after one hour the reaction was complete. After work-up and flash column chromatography, the pure 5′-*O*-dimethoxytrityl-$N^2$-diphenylacetyl-2′-deoxyguanosine-3′-*O*-(2-chlorophenyl phosphate) isobutyl ester was obtained. After standard removal of the protecting group [18], the crude mixture was purified by isocratic anion exchange chromatography (DEAE Sephacell, triethylammonium bicarbonate buffer 0·05 M); fractions containing the desired nucleotide with HPLC titre $\geqslant$ 95 per cent (RP18 Spherisorb column, $CH_3CN$ gradient in $KH_2PO_4$ 0·05 M buffer, pH = 4·5, $T$ = 45°C) were collected, co-evaporated with water several times to remove the buffer, and then transformed to the sodium salt (Dowex 50 W × 8 Ion exchange resin, $Na^+$ form), to afford 220 mg of the pure desired compound.

### 2.2. *Optical microscopy*

Microscopic observations of samples between slide and coverslip were performed with a Zeiss polarizing microscope equipped with a photocamera. Samples with a concentration gradient were obtained by peripheral evaporation of water solutions or by allowing water to penetrate the neat compound.

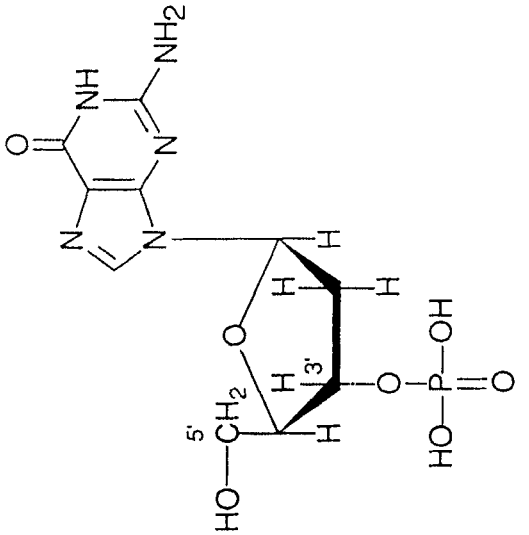

d(Gp)

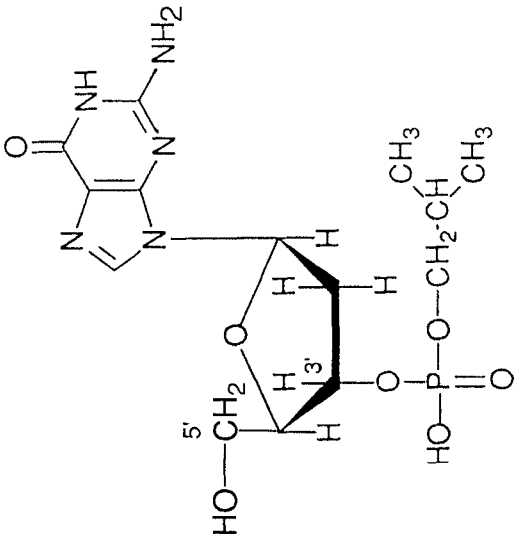

d(Gp)iBu

### 2.3. *X-ray diffraction*

X-ray diffraction experiments were performed using a 1·5 kW Ital-Structures X-ray generator equipped with a Guinier-type focusing camera operating under vacuum: a bent quartz crystal monochromator was used to select the Cu-$K_{\alpha 1}$ radiation ($\lambda = 1{\cdot}54$ Å). The samples were mounted in vacuum-tight cells with thin mica windows. In order to reduce the spottiness arising from possible macroscopic monodomains, the cells were continuously rotated during the exposure. The sample cell temperature was controlled with an accuracy of 0·5°C by using a circulating thermostat. The diffraction patterns were recorded on a stack of four Kodak DEF-392 films: densitometric traces were obtained by using a Joyce–Loebl microdensitometer and the relative intensities of the reflections were calculated as reported in [19]. X-ray high angle diffraction measurements were also performed using a rotating anode generator (Rigaku Denki RV 300) equipped with a powder diffractometer: Ni-filtered Cu-$K_{\alpha}$ radiation (average wavelength 1·54 Å) was used.

Samples were prepared by mixing the guanosine derivatives with fresh bidistilled water. The mixtures were left for at least 2 days at room temperature to avoid inhomogeneity: sometimes, but in many cases unsuccessfully (see below), longer times were used to reach equilibrium conditions. The final sample concentration was estimated by gravimetric analysis.

### 2.4. *Circular dichroism*

Circular dichroism (CD) spectra were recorded with a JASCO J-710 spectropolarimeter using a 0·001 cm path length cell with a water jacket connected to a Heto/Hetofrig thermostat.

## 3. Results and discussion

### 3.1. *Phase diagrams*

The ammonium salts of d(Gp) and d(Gp)iBu exhibit a very peculiar polymorphism. In addition to the previously described cholesteric phase (Ch) [14], three other liquid crystalline phases have been detected at room temperature as a function of the water content. All the observed phases are columnar. According to the model proposed for the other compounds investigated [10–12, 14–16], these derivatives also self-associate to form the Hoogsteen-bonded tetrameric arrangement reported in figure 1, in which four residues are related to each other by a 4-fold rotation axis [4, 13, 20]. The tetramers are piled on top of each other at a distance of about 3·4 Å to form the four-stranded columnar aggregates.

The analysis of the X-ray diffraction patterns (see below) gives the long range arrangement of the columnar elements at the different concentrations [21, 22]: in particular, two different 2-D hexagonal structures and a 2-D square structure have been detected. We will indicate by H, $H_b$ and Sq the two hexagonal and the square phases, respectively. The final phase dependences on concentration (at 25°C) are the following (concentration $c$ being expressed as weight of solute per weight of solution):

d(Gp) I 0·05 Ch 0·35 $H_b$ 0·58 Sq 0·68 H 0·90 C

d(Gp)iBu I 0·25 Ch 0·38 $H_b$ 0·52 Sq 0·70 H 0·90 C

It should be noticed that the hexagonal $H_b$ phase observed in the case of d(Gp)iBu is largely unstable. Samples prepared at concentrations intermediate between $c = 0{\cdot}38$ and $c = 0{\cdot}52$ show in fact the persistence of the cholesteric arrangement, and only in some cases the presence of the more ordered hexagonal $H_b$ phase.

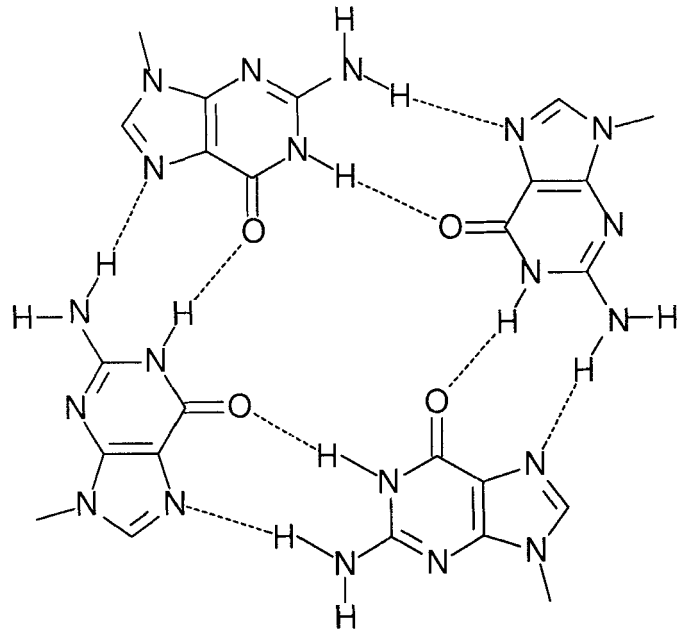

Figure 1. The tetrameric arrangement of guanine bases bonded in a Hoogsteen mode. A computer molecular display of a tetramer allows estimation of the 'diameter' of the unhydrated aggregate (including the phosphate/sugar groups) at about 24 Å.



### 3.2. *Optical microscopy observations*

Preliminary observations were carried out on d(Gp) and d(Gp)iBu samples with a concentration gradient obtained by peripheral evaporation or by allowing water to penetrate the neat sample. These observations show the presence of at least two liquid crystalline phases (see figure 2). The first one exists at high water content; on the basis of its typical texture, this phase has been described as cholesteric [10, 14]. The second phase exists at lower water content, and shows a herring-bone texture, typical of the hexagonal structure of guanosine derivatives [10, 11, 14, 16]. Similar textures have been reported also for the same phase in chromonics [17, 23] and DNA samples [24]. By further decreasing the water content, the texture does not show any observable modification: it remains birefringent and no phase transitions appear to take place. Considering the X-ray diffraction results (see below), it is evident that the textures relative to the differently ordered columnar phases ($H_b$, Sq and H) are very similar to or paramorphic with the first structure which is formed, so that phase transitions could not be detected by optical measurements.

Concerning the cholesteric phase, one important point must be stressed. In fact, in complete contrast to previous results [11, 14], we could not obtain, for either d(Gp) or d(Gp)iBu derivatives, the fingerprint texture, even after the samples had been kept in a magnetic field for a long time; no homogeneous planar texture could be obtained either. Considering the fact that the guanine tetrameric planes tend to align parallel to the magnetic field [11, 12, 14], this peculiar behaviour could indicate that the guanine residues which form the tetramers are not exactly perpendicular to the axis of the columnar aggregate. Therefore, the columnar aggregate could have a small diamagnetic anisotropy, or perhaps the columns are too entangled.

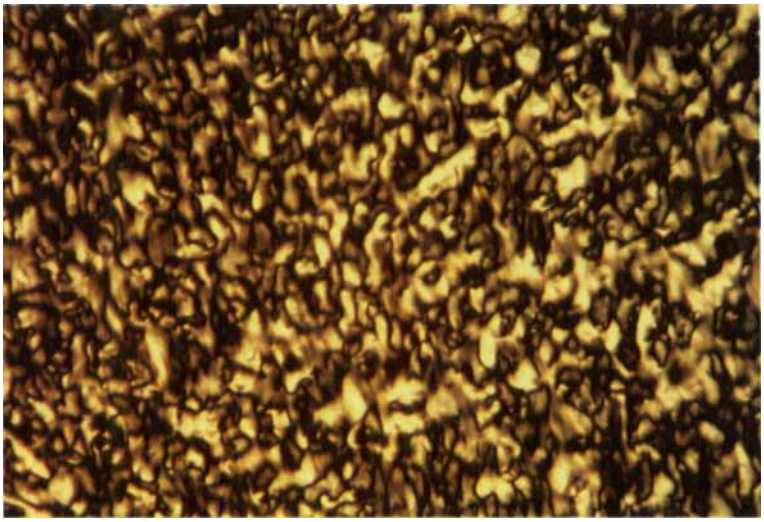

(*a*)

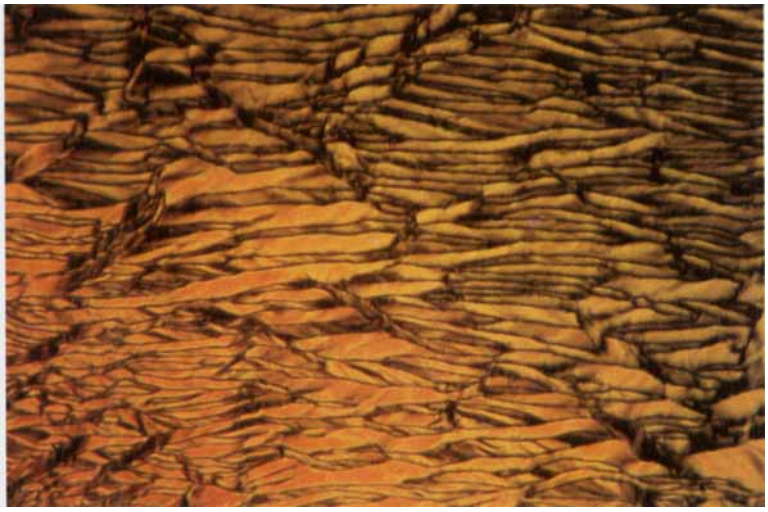

(*b*)

Figure 2. The schlieren texture of the cholesteric (*a*) and herringbone textures of the hexagonal (*b*) phases obtained from d(Gp)iBu in water. The photographs were taken with crossed polarizers on samples with a coverslip (original magnification $\times 250$).

### 3.3. *Circular dichroism: the handedness of the columnar aggregates*

The circular dichroism technique is very sensitive to stereochemical variations. It is therefore ideal for tracing the aggregation process from isolated chiral molecules to supramolecular aggregates and finally to cholesteric mesophases; also the handedness of the cholesteric phase may be deduced by CD.

Figure 3 shows three typical CD spectra of d(Gp) ammonium salt at $c = 0{\cdot}04$ at different temperatures. At the lowest temperature (curve (*a*)), the spectrum is intense, has the same sign over the spectral range investigated and a profile similar to that of the absorption spectrum with maxima at *c.* 210 and 245 nm and a shoulder at *c.* 280 nm. This curve is related to the formation of the cholesteric phase [25]. On increasing the temperature, the intensity of the spectrum decreases, but the profile remains the same up to a critical value of temperature, where a sharp modification of both profile and intensity occurs. The spectrum observed (curve (*b*)) is characterized by a negative maximum at 260 nm, a positive shoulder at *c.* 235 nm and also a positive maximum at 215 nm. This curve represents the CD spectrum of the aggregated form of d(Gp) in isotropic solution. By further increasing the temperature, the columnar aggregates appear to break: the melting profile of the aggregates can be followed, and finally a weak CD spectrum characteristic of an isolated molecule is obtained (curve (*c*)). A similar variation of the CD spectrum could be obtained by increasing the water content at fixed temperature.



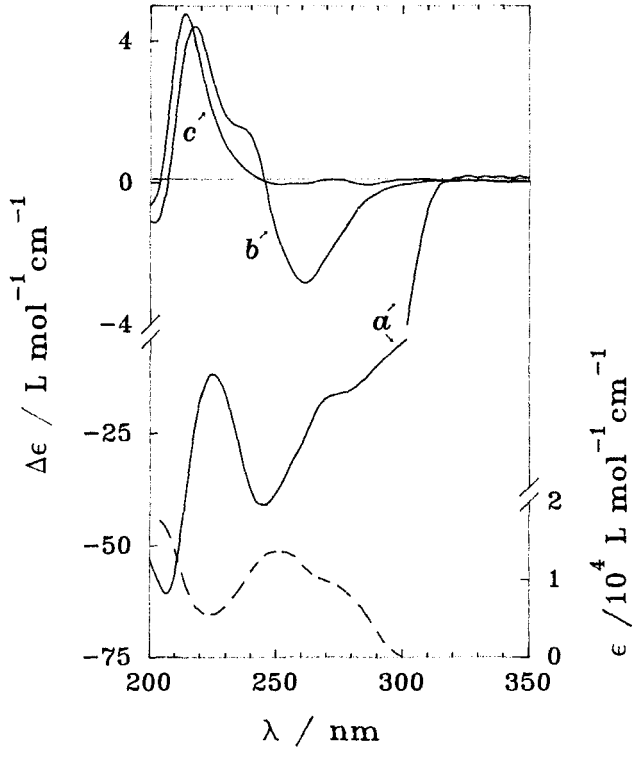


Figure 3. The absorption (dashed line) and CD (full lines) spectra of d(Gp) in water, $c = 0{\cdot}04$. Curves (*a*) (*b*) and (*c*) are recorded at 1, 15 and 40°C, respectively.

In order to solve the problem of the handedness of the aggregate in solution, a comparison with the CD results of poly(G) is useful. Poly(G) is known to form a right-handed four-stranded helix and its CD spectrum is characterized by a positive exciton couplet around 250 nm (positive band at 260 nm and negative band at 235 nm) [26]. Recently, CD calculations on stacked arrays of guanosine tetramers based on the exciton approximation have been reported by some of us [26]; the calculated spectrum reproduces very well the experimental spectrum of poly(G). Basically, the diagnostic signal for the handedness is the couplet centred at *c.* 250 nm, whose sign is directly related to the handedness of the aggregate. In the present case, the negative exciton couplet at *c.* 250 nm (negative band at 260 nm and positive shoulder at 235 nm), evident in curve (*b*), indicates a left-handed helix made up of piled rotated tetramers.

Going back to curve (*a*) of figure 3, the handedness of the cholesteric phase may also be inferred. It can be correlated with the CD spectrum by means of the following equation [27, 28]

$$(OD_L - OD_R) = \frac{p\nu_j^3 \Delta n (OD_\perp - OD_\parallel)_j}{2(\nu_j^2 - \nu_0^2)}, \tag{1}$$

where $(OD_L - OD_R)_j$ is the CD at frequency $\nu_j$, $\nu_0$ is the frequency of the selective reflection which is correlated to the cholesteric pitch $p$ (positive for a right-handed helix), $\Delta n$ is the optical anisotropy, and $(OD_\perp - OD_\parallel)_j$ is the linear dichroism of the helix-building objects.

Therefore, in our case, assuming a model of stacked arrays of Hoogsteen-bonded guanosines [11, 14], negative CD is related to a left-handed cholesteric superhelix.

The isobutyl ester derivative shows a similar ability to form an aggregate composed of Hoogsteen-bonded guanosine tetramers in a left handed helical stack. Figure 4 reports a spectrum (curve (*a*)) showing again a negative exciton couplet centred at *c.* 250 nm that disappears when the temperature is increased above its melting value (curve (*b*)).

To summarize, CD spectra for both compounds in isotropic solution support the model of aggregates composed of a helical stacking of Hoogsteen-bonded guanosine tetramers.

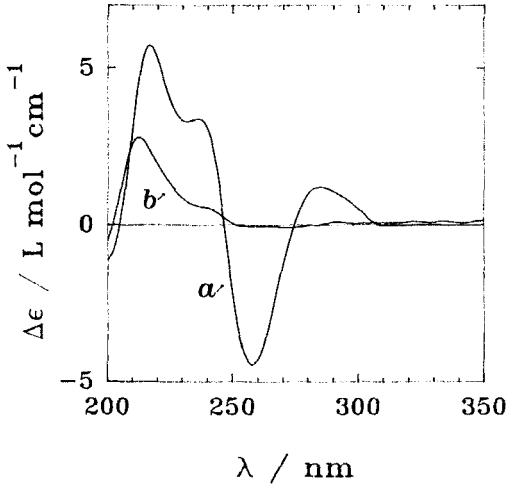


Figure 4. The CD spectra of d(Gp)iBu in water (KCl 0·05 M), $c = 0{\cdot}01$, recorded at (*a*) 1°C and (*b*) 80°C.

3.4. *X-ray diffraction measurements: the structure of the columnar phases*

The structure of the different phases has been derived from the analysis of the corresponding X-ray diffraction profiles. From a qualitative point of view, both investigated compounds show equivalent structural behaviour. In the following paragraphs, we discuss the results relating to the d(Gp) compound, while the data concerning the d(Gp)iBu derivative will be presented in a separate section.

According to the structural properties of thermotropic columnar liquid crystals [29], and in keeping with a rule fulfilled by the guanosine derivatives investigated [11, 12, 14, 16], a narrow band centred in the high angle X-ray diffraction region at about $s=(3{\cdot}4\,\text{Å})^{-1}$ ($s$ being defined as $2\sin\theta/\lambda$, where $2\theta$ is the scattering angle, and $\lambda$ the X-ray wavelength) is indicative of a columnar liquid crystalline phase. This reflection is related to the nature of the intracolumnar order of the structure elements [29]. In our systems, the columnar aggregates are composed of a stacked array of guanosine tetramers, equally spaced at a distance of about 3·4 Å. In figure 5, the tetramer stacking distance $\Delta$ observed in the case of d(Gp) derivative is plotted as a function of concentration: this distance does not change even when phase boundaries are crossed.

It should also be noticed that the $(3{\cdot}4\,\text{Å})^{-1}$ narrow band is not detectable in the diluted isotropic solutions, even if for other derivatives the presence of short rods has been inferred by neutron small-angle scattering measurements [15]. By contrast, a large number of strong and very narrow Bragg reflections characterizes the high angle X-ray diffraction region when the sample is in the crystalline (hydrated) state.

3.4.1. *The cholesteric Ch phase*

At high dilution, when the samples observed by optical microscopy show the cholesteric texture, the X-ray diffraction profiles are characterized by two reflections. The first one is centred in the low angle region and appears as a diffuse band: its position strongly depends on the water content (see table 1). The second reflection is the narrow $(3{\cdot}4\,\text{Å})^{-1}$ band, the position and shape of which is independent of the sample concentration. Such a profile confirms that we are dealing with a cholesteric phase similar to those previously observed in all the guanosine derivatives investigated [11, 14]. This phase is characterized by columns arranged in a helicoidal fashion: the observed low angle peak refers to the mean distance between neighbouring cylinders,

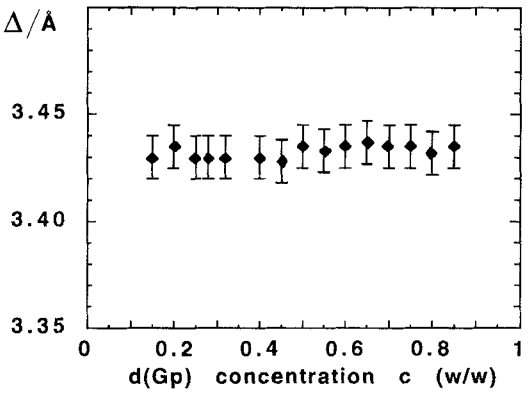


Figure 5. The variation of distance $\Delta$ between stacked d(Gp) tetramers, obtained from the position of the narrow peak in the high angle X-ray diffraction profile, as a function of the concentration at 25°C.

Table 1. X-ray diffraction data analysis: indexing of the experimental patterns observed for d(Gp) samples with different water concentrations at 25°C. In the first line of each section of the table, the water concentration $c$ (w/w) and the dimension of the 2-D unit cell of each sample are reported. $s$ (in $Å^{-1}$, see the definition in the text) is the reciprocal spacing of the reflections with $h,k$ indices, obs refers to the observed spacing, while clc refers to those calculated for the 2-D hexagonal and square phases, using the reported lattice parameters.

Hexagonal H phase

| $c, a$ | 0·85, 27·0 Å | | 0·80, 28·4 Å | | 0·75, 30·3 Å | | 0·70, 31·8 Å | |
|---|---|---|---|---|---|---|---|---|
| $h,k$ | $s_{clc}$ | $s_{obs}$ | $s_{clc}$ | $s_{obs}$ | $s_{clc}$ | $s_{obs}$ | $s_{clc}$ | $s_{obs}$ |
| 1,0 | 0·043 | 0·043 | 0·041 | 0·041 | 0·038 | 0·038 | 0·036 | 0·036 |
| 2,1 | 0·074 | — | 0·070 | 0·071 | 0·066 | 0·066 | 0·063 | 0·063 |
| 2,0 | 0·085 | — | 0·081 | — | 0·076 | — | 0·073 | — |
| 3,1 | 0·113 | — | 0·107 | — | 0·101 | 0·101 | 0·096 | 0·096 |
| 3,0 | 0·128 | 0·129 | 0·122 | 0·122 | 0·114 | — | 0·109 | — |
| 4,2 | 0·148 | 0·149 | 0·141 | 0·140 | 0·132 | 0·131 | 0·126 | 0·125 |
| 4,1 | 0·154 | 0·153 | 0·146 | 0·146 | 0·137 | 0·137 | 0·131 | 0·131 |

Square Sq phase

| $c, a$ | 0·65, 30·1 Å | | 0·60, 30·9 Å | |
|---|---|---|---|---|
| $h,k$ | $s_{clc}$ | $s_{obs}$ | $s_{clc}$ | $s_{obs}$ |
| 1,0 | 0·033 | 0·033 | 0·032 | 0·031 |
| 1,1 | 0·047 | 0·047 | 0·046 | 0·046 |
| 2,0 | 0·066 | 0·065 | 0·065 | 0·064 |
| 2,1 | 0·074 | 0·072 | 0·072 | — |
| 2,2 | 0·094 | — | 0·092 | — |
| 3,0 | 0·100 | — | 0·097 | — |
| 3,1 | 0·105 | — | 0·102 | — |
| 3,2 | 0·120 | — | 0·117 | — |
| 4,0 | 0·133 | 0·133 | 0·129 | 0·130 |
| 4,1 | 0·137 | 0·138 | 0·133 | 0·134 |
| 3,3 | 0·141 | 0·143 | 0·137 | 0·137 |

Hexagonal $H_b$ phase

| $c, a$ | 0·55, 44·3 Å | | 0·50, 44·9 Å | | 0·45, 47·8 Å | | 0·40, 50·7 Å | |
|---|---|---|---|---|---|---|---|---|
| $h,k$ | $s_{clc}$ | $s_{obs}$ | $s_{clc}$ | $s_{obs}$ | $s_{clc}$ | $s_{obs}$ | $s_{clc}$ | $s_{obs}$ |
| 1,0 | 0·027 | 0·027 | 0·026 | 0·026 | 0·024 | 0·024 | 0·023 | 0·023 |
| 2,1 | 0·046 | 0·045 | 0·045 | 0·045 | 0·042 | 0·042 | 0·039 | — |
| 2,0 | 0·052 | 0·052 | 0·051 | — | 0·048 | — | 0·046 | 0·046 |

Cholesteric Ch phase

| $c, a$ | 0·32, 49·2 Å | 0·28, 51·9 Å | 0·25, 54·1 Å | 0·20, 57·0 Å | 0·15, 65·0 Å |
|---|---|---|---|---|---|
| | $s_{obs}$ | $s_{obs}$ | $s_{obs}$ | $s_{obs}$ | $s_{obs}$ |
| | 0·020 | 0·019 | 0·018 | 0·017 | 0·015 |

which obviously changes as a function of concentration. The narrow band at about $(3{\cdot}4\ \text{Å})^{-1}$ indicates the usual tetramer stacking distance. However, as reported above, microscopic observation indicates that even prolonged exposure to a magnetic field is not sufficient to align the cholesteric helix. X-ray diffraction experiments confirm that with a magnetic field it is not possible to obtain oriented samples.

3.4.2. *The hexagonal H phase*

A columnar hexagonal liquid crystalline phase exists between about $c=0{\cdot}68$ and $c=0{\cdot}90$. The low angle X-ray diffraction profile is characterized by an unusual number of narrow reflections (almost 7 Bragg peaks), which indicates that the phase is highly regular (see table 1). The peak positions are in the ratio $1, \sqrt{3}, \sqrt{4}\ldots$ and are compatible with a 2-D hexagonal lattice of p6m symmetry (space group No. 17 of the International Tables of Crystallography [21]). The equation which defines the spacing of the reflections is in fact [21, 22]

$$s_{hk}=\frac{2}{\sqrt{3}}\frac{\sqrt{(h^2+k^2-hk)}}{a}, \tag{2}$$

where $a$ is the unit cell dimension and $h, k$ the Miller indices of the reflection.

As the narrow band at $s=(3{\cdot}4\ \text{Å})^{-1}$ is still present, it appears reasonable to assume the same model for this phase that was previously proposed for the other guanosine derivatives [11, 14], i.e. parallel columnar aggregates, formed by piled tetramers, packed in a hexagonal array (see figure 6(*A*)). Each aggregate is surrounded by six others, at a distance $D$ equal to the unit cell dimension. It is evident that the projection of the rod in the plane of the 2-D cell shows neither the 6-fold symmetry required by the lattice nor a higher one [21]. This symmetry is presumably reached through an orientational disorder of the tetramers due to the free $2\pi$ rotations of the columns along their long axis. Moreover, the absence of any other diffraction indicates that no long range column–column correlation of the tetramer position exists: the structural elements may freely translate in a direction perpendicular to the 2-dimensional hexagonal cell. However, X-ray diffraction investigation on the structure of guanosine fibres [30] as well as computer molecular models [20] indicate that the stacking is helical, i.e. the tetramers are not piled in register, but are instead rotated with respect to each other to create an internal helix. CD measurements confirm the presence of the internal helix in the isotropic phase of d(Gp) (see above), as well as in the other previously investigated guanosine derivatives [11, 14]. We consider that it is reasonable to assume that the internal helix exists also in the columnar aggregates which form the hexagonal structure.

As reported in table 1, the hexagonal unit cell dimension changes continuously as a function of the sample concentration. As usual in chromonic phases [31] (see also [22] for the corresponding behaviour exhibited by lyotropic phases), the distance between the rods increases as the water content increases. By assuming that water does not penetrate the rods and that the columns have a circular section and are infinitely long (as could be expected, if the location of this phase in the phase diagram is considered [12, 32], see also below), the following equation could be used to calculate the radius of the tetramers

$$R=\sqrt{\left(\frac{\sigma C_{v,d(Gp)}}{\pi N}\right)}, \tag{3}$$

Table 2. Structure parameters of d(Gp) samples in the hexagonal H phase. $c$ is the water concentration (w/w); $a$ is the unit cell dimension; according to the International Tables [21], the Pos.,sym column gives the Wyckoff notation and the point symmetry of the special positions where the columnar aggregates are centred; $N$ is the number of rods in the unit cell; $R$ is the radius of the section, supposed circular, of the columnar aggregates, assumed to be infinitely long, calculated supposing that water does not penetrate the rods, as reported in the text.

| $c$ | Space group | $a$/Å | Pos.,sym | $N$ | $R$/Å |
|---|---|---|---|---|---|
| 0·85 | H(p6m) | 27·0 | $a$, 6mm | 1 | 12·6 |
| 0·80 | H(p6m) | 28·4 | $a$, 6mm | 1 | 12·9 |
| 0·75 | H(p6m) | 30·3 | $a$, 6mm | 1 | 12·7 |
| 0·70 | H(p6m) | 31·8 | $a$, 6mm | 1 | 12·9 |

Table 3. Structure parameters of d(Gp) samples in the square Sq phase. $\alpha$ is the average tilt angle formed by the guanosine residues inside the tetrameric plane with respect to the normal to the columnar long axis; $\alpha$ has been calculated by using $\alpha = \cos^{-1}(R/12{\cdot}8)$, where 12·8 Å is the expected rod radius. Other notations and symbols are as in table 2.

| $c$ | Space group | $a$/Å | Pos.,sym | $N$ | $R$/Å | $\alpha$/° |
|---|---|---|---|---|---|---|
| 0·65 | Sq(p4) | 30·1 | $a$, 4 | 1 | 12·6 | 10·1 |
| 0·60 | Sq(p4) | 30·9 | $a$, 4 | 1 | 12·3 | 16·0 |



where $\sigma$ ($\sigma = a^2\sqrt{3}/2$) is the area of the 2-D hexagonal unit cell, $N$ the number of columns per unit cell ($N = 1$) and $C_{v,d(Gp)}$ the guanosine volume concentration calculated by considering 1·00 and 0·651 $cm^3\,g^{-1}$ as the specific volume of water and of the d(Gp) compound, respectively [11, 14, 22]. The results, reported in table 2, indicate a roughly constant radius of about 12·8 Å, in agreement with molecular calculations [20] and the previous analysed guanosine systems [11, 14].

3.4.3. *The square Sq phase*

A different chromonic phase is observed in the concentration region between $c = 0{\cdot}68$ and $c = 0{\cdot}58$. The presence of the narrow $(3{\cdot}4\,\text{Å})^{-1}$ band indicates again a columnar arrangement of the structural elements. The low angle X-ray diffraction profile is characterized by several sharp peaks (see table 1), whose spacings are in the ratio $1:\sqrt{2}:\sqrt{4}\ldots$, which corresponds to the packing of infinite cylinders on a two-dimensional square lattice. In this case, the equation which gives the spacing of the observed reflections reads

$$s_{hk} = \frac{\sqrt{(h^2+k^2)}}{a}. \tag{4}$$

As in the hexagonal phase, the absence of any other diffraction confirms that there is no long range correlation in the longitudinal positions of the columns: the structural elements are able to slide with respect to each other.

The observed X-ray diffraction profile is compatible with the 2-dimensional p4 space group (No. 10) [21]. In particular, one columnar structural element per unit cell is centred at a position of co-ordinates 0, 0, named $a$ in the International Tables of Crystallography [21]. Considering the point symmetry, we can reasonably assume, as before, that the columns are free to rotate around their long axes, so that the projection

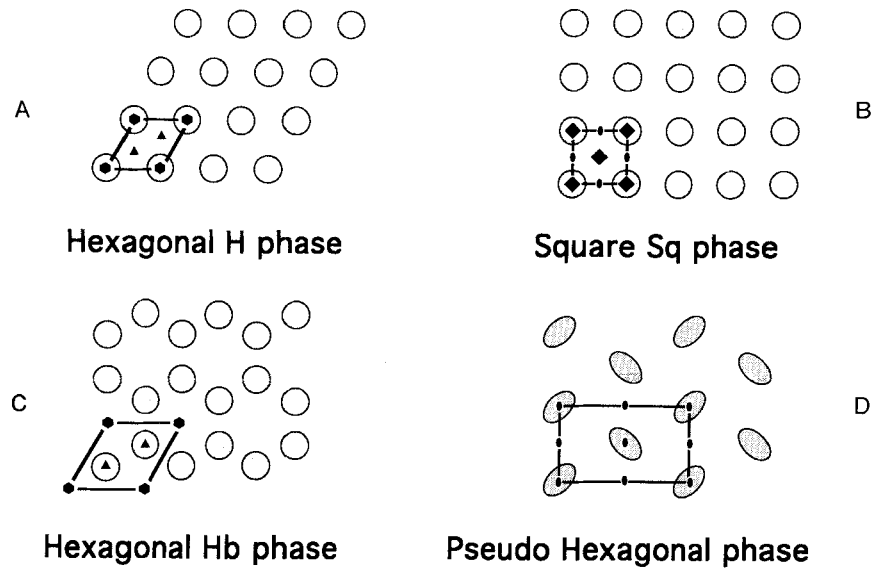


Figure 6. The representation of the columnar packing described in the text for the hexagonal, square, hexagonal $H_b$ and pseudo-hexagonal phases. The heavy black lines mark the unit cells; some of the symmetry elements are also shown. As required by the point symmetry, the section of the columns in the pseudo-hexagonal phase is represented as elliptical.



of the columns in the plane of the 2-D unit cell is circular; this is compatible with the p4 lattice [21]. The structure is represented in figure 6 (*B*). It should be noticed that each columnar aggregate is surrounded by four other columns, at a distance $D = a$.

Assuming as above that water does not penetrate the rods and that the structural elements have a circular section and are infinite in length, the dimension of the tetramer can be calculated. The results obtained by using equation (3), where $\sigma$ is now the area of the square unit cell ($\sigma = a^2$) and $N$ is equal to 1, are reported in table 3. Considering the expected dimension of the columns [11, 14, 20] and the values observed in the neighbouring hexagonal phase, the agreement is satisfactory.

3.4.4. *The hexagonal $H_b$ phase*

This phase extends in the concentration region between $c = 0{\cdot}58$ and $c = 0{\cdot}35$. The presence of the narrow $(3{\cdot}4\,\text{Å})^{-1}$ band in the high angle X-ray diffraction profile indicates once more that the phase is columnar. The low angle diffraction is characterized by three reflections at most, whose spacing positions are in the ratio $1 : \sqrt{3} : \sqrt{4}$. Once again, the absence of any extra peak in the X-ray diffraction patterns indicates that no long range column–column correlation exists. The observed profile is therefore compatible with a packing of columns in a 2-dimensional hexagonal lattice [21]. However, the structure seems different from the one described above (figure 6 (*A*)): in fact, by using equation (3) (with $\sigma = a^2\sqrt{3}/2$ and $N = 1$) and with the usual hypothesis that the columnar aggregates are infinite and have a circular section, a radius of about 15 Å has been obtained (see table 4, second block). This value does not agree with the expected dimension of the tetramers, which reasonably cannot exceed 13 Å [11, 14, 20].

Therefore, other structural models has been considered. In the best one, there are two infinite columns packed in the p6m 2-D hexagonal space group (No. 17) [21], but

Table 4. Structure parameters of d(Gp) samples in the hexagonal $H_b$ phase. Notations and symbols are as in tables 2 and 3. In the second and third section of the table, the structural parameters derived from the other possible packing models discussed in the text are reported.

| $c$ | Space group | $a$/Å | Pos.,sym | $N$ | $R$/Å | $\alpha$/° |
|---|---|---|---|---|---|---|
| 0·55 | H(p6m) | 44·3 | *b*, 3m | 2 | 10·9 | 31·6 |
| 0·50 | H(p6m) | 44·9 | *b*, 3m | 2 | 10·5 | 34·8 |
| 0·45 | H(p6m) | 47·8 | *b*, 3m | 2 | 10·5 | 34·8 |
| 0·40 | H(p6m) | 50·7 | *b*, 3m | 2 | 10·4 | 35·6 |
| 0·55 | H(p6m) | 44·3 | *a*, 6mm | 1 | 15·5 | |
| 0·50 | H(p6m) | 44·9 | *a*, 6mm | 1 | 14·8 | |
| 0·45 | H(p6m) | 47·8 | *a*, 6mm | 1 | 14·8 | |
| 0·40 | H(p6m) | 50·7 | *a*, 6mm | 1 | 14·7 | |
| 0·55 | PsH(pgg) | 44·3 | *a*, 2 | 2 | 15·5 | |
| 0·50 | PsH(pgg) | 44·9 | *a*, 2 | 2 | 14·8 | |
| 0·45 | PsH(pgg) | 47·8 | *a*, 2 | 2 | 14·8 | |
| 0·40 | PsH(pgg) | 50·7 | *a*, 2 | 2 | 14·7 | |



centred on the special positions *b* (co-ordinates 1/3, 2/3 and 2/3, 1/3) of 3m point symmetry. It could be expected that in this case also, the columns are able to rotate around their long axis, so that the shape of the projection of the columns in the plane of the 2-D unit cell will be compatible with the point symmetry. We have named this phase $H_b$: its unusual columnar packing is schematically depicted in figure 6 (*C*). Each column is surrounded by three other rods: the distance $D$ between the closest neighbouring aggregates is given by $a/\sqrt{3}$. The dimensions of the tetramer, which have been determined by using equation (3) (with $\sigma = a^2\sqrt{3}/2$ and $N = 2$) and which are reported in table 4 (first block), appear in good agreement with the ones observed in the neighbouring phases.

It is interesting to discuss also a second model, which is compatible with the scattering data, but does not agree with the expected tetramer dimension. This model consists of parallel columns packed in a two-dimensional (pseudo-hexagonal) rectangular lattice of p2gg symmetry (space group No. 8) [21, 29, 33, 34]. In such a structure (lattice parameters $a = b\sqrt{3}$, where $a$ and $b$ are the minor and the major sides of the rectangular unit cell, respectively), the condition limiting possible reflections is

$$s_{hk} = \frac{\sqrt{(3h^2 + k^2)}}{b}. \tag{5}$$

Consequently, the spacing ratios of the three observed reflections are: $\sqrt{4} : \sqrt{12} : \sqrt{16}$. In this model, there are two rods per unit cell, centred on the 2-fold axis (position *a* of co-ordinates 0, 0; 1/2, 1/2) and packed according to a herring-bone scheme, as reported in figure 6 (*D*). Noteworthy, this packing is possible only if the columns have an ellipsoidal section (i.e. if the rod projection in the unit cell plane shows a 2-fold rotation symmetry) and if this anisotropic shape does not permit the $2\pi$ rotation of the aggregates along their long axes. The elongated sectional shape could correspond to a tilted arrangement of the tetramer plane with respect to the long axis of the rods [33, 34]. However, even considering infinitely long columns, the dimensions of the tetramer, calculated by using equation (3) where $\sigma = (a\,b)$ and $N = 2$, appear incompatible with the expected rod section (see table 4, third block).

3.4.5. *The electron density maps*

Electron density maps have been determined for the three 2-D phases, and unambiguously confirm the suggested columnar packings. In particular, the phase problem has been solved considering the continuous change of the observed intensity of the low angle X-ray diffraction peaks as a function of the water content (for more detail, see [11, 14]). In fact, within the same phase, one could expect that, at all concentrations, the electron density distribution of the cylinders will remain fairly constant and that the increased water content will only increase the separation between the columns. According to the notion that in these conditions the structure factors sample a unique continuous curve, we expect the amplitudes of the observed reflections to change continuously as a function of the $s$ values of the reflections. From the position of the zeros, the signs of the corresponding structure factors may be derived. Figure 7 shows that, in all three phases investigated, the data fulfil this expectation and specify the sign of the structure factors. It is interesting to note that the intensity cut-off shifts to smaller $s$ values as the unit cell dimension increases, indicating that the lattice disorder increases with increasing water content.

Three maps relative to three different d(Gp) concentrations and calculated following the hexagonal and square 2-D symmetries, are reported in figure 8. They clearly show the electron dense columnar projection, roughly circular in all the three phases (note 1). The rods appear surrounded by a smooth region of lower electron density, which is associated with water. The small satellite holes of lower electron density around each major peak in the map relative to the hexagonal H phase could indicate some rotational positioning of the tetramers; however, we consider that they are merely series termination features caused by the small number of Fourier terms used in the calculation. Note finally that the agreement between the radii of the columnar cross-section, directly measured from the electron density distribution maps, and the expected tetramer dimension is excellent.



### 3.5. *The d(Gp) isobutyl ester*

The d(Gp)iBu derivative shows very similar structural behaviour. X-ray diffraction experiments and optical microscopy confirm the existence of a cholesteric phase at low concentration, which, as in the case of d(Gp), could not be aligned by even long exposure to a magnetic field. At higher concentrations, a hexagonal $H_b$, a square Sq and a hexagonal H phase were also formed. All these liquid crystalline structures are columnar, as indicated by the rather narrow reflection at about $s=(3{\cdot}4\,\text{Å})^{-1}$ observed in the high angle X-ray diffraction profiles. In consequence, the structural models which appear consistent with the experimental observations are based on the packing of columnar aggregates. The lattice dimensions and symmetries and the structural data obtained from the analysis of the X-ray diffraction profiles are listed in table 5.

The structural parameters appear very similar to those observed in the d(Gp) derivative; however, the concentrations at which phase transitions occur are not the same, indicating that the ability of this derivative to form liquid crystalline phases is different. In particular, the fact that the cholesteric phase is observed only at a relatively high concentration ($c=0{\cdot}25$), while CD measurements show that supramolecular aggregates are already present at $c=0{\cdot}05$, suggests that the growth of the columns in the isotropic phase proceeds with some difficulty. It should also be noted that the hexagonal $H_b$ packing appears to be quite unstable: in many cases, in fact, the cholesteric arrangement has been observed to persist until a direct transition to the square phase. A possible explanation of this behaviour could be in terms of the

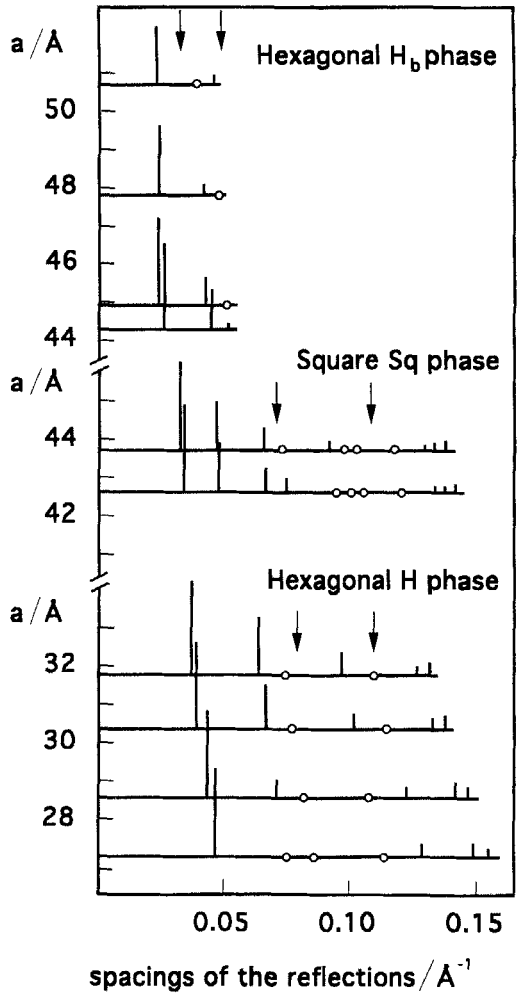


Figure 7. Analysis of the amplitude of the reflections observed for d(Gp) in the different phases. Each experiment is identified by a horizontal line, whose ordinate is the lattice parameter *a*. The vertical bars are roughly proportional to the observed amplitudes of the reflections: the open circles represent reflections whose intensities are too weak to be measured. The general trend of the three phases is consistent with the notion that, in each case, the structure factors sample a unique continuous curve, whose zeros are shown by the vertical arrows.

lengthening of the aggregates, which can proceed only slowly in the cholesteric phase, hence retarding the transition to the 2-D phase (see also the following paragraph).

### 3.6. *The ordering of the columns and the phase sequence*

Contrary to generally accepted opinion, in the present case the lyotropic phase sequence does not appear to be directly related to changes in the shape of the columns [34] (see also [33]). As reported above, we suppose that the symmetry required by the different observed lattices is reached through an orientational disorder of the section of the columnar aggregate along their long axes. In fact, the tetramers have a 4-fold rotation axis, but the 6-fold symmetry in the hexagonal H phase, as well as the 3-fold symmetry in the $H_b$, phase is reached by $2\pi$ rotations of the columns along their long

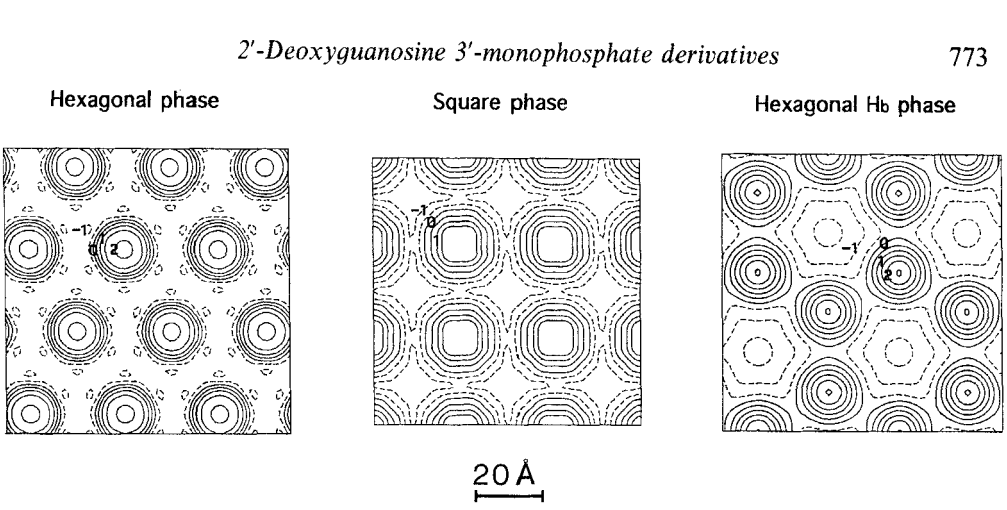


Figure 8. Electron density distributions of the hexagonal, square and hexagonal $H_b$ phases of d(Gp) at concentrations $c$ equal to 0·75. 0·65 and 0·55, respectively. The electron density scale is arbitrary: the intensity data have been normalized so that the sum of the scattered intensity is equal to 1 (see [10] and [13]). The density lines are equally spaced, with an increment of 0·5: negative levels, which, following our normalization, correspond to the region of lower electron density, are dotted, while the positive ones, which correspond to the regions of higher electron density, are continuous. Note that, in the three maps, the contour level in the centre of the rod sections corresponds to the maximum of electron density. The structure factors $F(h,k)$ are: in the hexagonal H phase, $F(1,0)=0{\cdot}395$, $F(2,1)=0{\cdot}040$, $F(2,0)=0{\cdot}0$, $F(3,1)=-0{\cdot}062$, $F(3,0)=0{\cdot}0$, $F(4,2)=0{\cdot}028$, $F(4,1)=0{\cdot}020$; in the square Sq phase, $F(1,0)=0{\cdot}468$, $F(1,1)=0{\cdot}148$, $F(2,0)=0{\cdot}066$, $F(2,1)=-0{\cdot}033$, $F(2,2)=0{\cdot}0$, $F(3,0)=0{\cdot}0$, $F(3,1)=0{\cdot}0$, $F(3,2)=0{\cdot}0$, $F(4,0)=-0{\cdot}033$, $F(4,1)=-0{\cdot}023$, $F(3,3)=-0{\cdot}015$; in the hexagonal Hb phase, $F(1,0)=-0{\cdot}331$, $F(2,1)=0{\cdot}234$, $F(2,0)=-0{\cdot}052$.



Table 5. Structure parameters of d(Gp)iBu samples in the H, Sq, $H_b$ and Ch phases. Δ is the tetramer stacking distance as obtained from the position of the high angle peak observed in X-ray diffraction profiles. Other notations and symbols are as in tables 2, 3 and 4.

| $c$ | Space group | $a$/Å | Pos.,sym | $N$ | $R$/Å | α/° | Δ/Å |
|---|---|---|---|---|---|---|---|
| 0·85 | H (p6m) | 27·0 | $a$, 6mm | 1 | 12·8 | — | 3·423 |
| 0·80 | H (p6m) | 28·6 | $a$, 6mm | 1 | 12·7 | — | 3·427 |
| 0·75 | H (p6m) | 29·8 | $a$, 6mm | 1 | 12·8 | — | 3·418 |
| 0·65 | Sq (p4) | 30·3 | $a$, 4 | 1 | 12·6 | 8·8 | 3·435 |
| 0·63 | Sq (p4) | 30·5 | $a$, 4 | 1 | 12·5 | 12·5 | 3·432 |
| 0·60 | Sq (p4) | 30·8 | $a$, 4 | 1 | 12·2 | 17·8 | 3·423 |
| 0·55 | Sq (p4) | 31·0 | $a$, 4 | 1 | 11·6 | 24·5 | 3·434 |
| 0·50 | H (p6m) | 46·6 | $b$, 3m | 2 | 10·9 | 31·8 | 3·442 |
| 0·40 | H (p6m) | 52·1 | $b$, 3m | 2 | 10·6 | 33·7 | 3·377 |
| 0·50 | Ch | 41·2 | | | | | 3·423 |
| 0·45 | Ch | 42·1 | | | | | 3·430 |
| 0·32 | Ch | 48·6 | | | | | 3·420 |
| 0·25 | Ch | 54·1 | | | | | 3·423 |

axes. In the square Sq phase, which is intermediate between the H and $H_b$ phases, we assume that rotation is also allowed, so that, according to what was observed in the electron density maps, the projection of the columns in the unit cell plane in this case also has a circular shape.

However, such phase behaviour has never been observed in the other investigated derivatives, which, as a rule exhibit a direct hexagonal to cholesteric phase transition [11, 14]: the esterification of the OH group in the 3′-position has a peculiar effect in stabilizing the columnar packing and we suppose that the observed phase sequence is mainly determined by the occurrence of strong short-range intercolumnar interactions.

In order to understand the origin of such a peculiar polymorphism, it is relevant to analyse the correlations between the columns in the different phases and in particular when the sample composition changes. In the H, Sq and $H_b$ phases, each columnar aggregate is surrounded by 6, 4 and 3 columns, respectively. However, the 2-D pair correlation functions, obtained by weight averaging the number of columns observed at the same distance in the 2-D plane, present a very similar shape in the three ordered phases: as expected, the fitting parameters indicate that the columnar packing in the hexagonal H phase is the most dense, and that the packing density decreases on going from the hexagonal H to the square Sq and from the square Sq to the hexagonal $H_b$ phase. Moreover, it must be noticed that the analysis of the 2-D pair correlation functions also indicates that, with respect to the other phases, in the $H_b$ structure the long-range columnar order decreases faster.

The short-range correlations could easily be analysed considering, in the different phases, the distance between the nearest neighbouring columns: in particular, figure 9 shows its variation as a function of the guanosine derivative concentration. Within each phase region, this distance increases with dilution, but the sawtooth nature of the graph implies that there is a limiting separation of the columns (a centre to centre distance of about 30 Å). The change from the H phase, where each column has 6 neighbours, to the square phase, where each has 4, to the $H_b$ phase, where each has 3, is an attempt by the structure to preserve this separation. Considering that the radius of the columnar cross-section, calculated as reported above, ranges between 12·9 Å and 10·4 Å (see tables 2, 3, 4 and 5), it appears that phase transformations occur systematically when the water layer between the columns is bigger than *c.* 6 Å. When

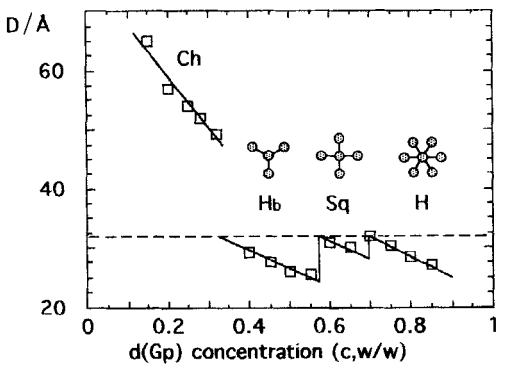


Figure 9. Variation of the distance between the first neighbouring columns observed in the different phases of d(Gp) as a function of concentration. Note the discontinuities in correspondence to the phase transitions. The reported lines are guides to the eyes.

other 2-D rearrangements are no longer possible, the cholesteric phase is then formed. In the case of the d(Gp)iBu derivative, the metastability of the hexagonal $H_b$ phase could be explained considering that a fairly large intercolumnar distance is reached in the square Sq phase. In these conditions, the short-range interactions may be too weak to force the system to assume a 2-D ordered packing, and thereby the cholesteric phase appears. However, the hexagonal $H_b$ phase could eventually also be formed, for example, as a consequence of a non-uniform hydration of the sample, which could prevent the rearrangement of the columns in a helicoidal fashion.

The analysis of the variation of the unit cell dimension as a function of the guanosine volume concentration can also give information about the length of the columnar aggregates [32, 35]. In fact, it has been predicted theoretically [36] that the exponent $-1/3$ must characterize the $a$ versus $C_v$ curves in the case of finite objects, with a water volume around the particles decreasing in all three dimensions; however, the exponent $-1/2$ is observed in the case of 'infinite' objects (i.e. infinitely long aggregates with interparticle distance decreasing in a plane). In both the derivatives investigated here, the functional behaviour expected for aggregates of infinite length has been observed in the H, Sq and $H_b$ phases (see figure 10, relative to the d(Gp) sample). By contrast, the exponent of the curve $a$ versus $C_v$ for the cholesteric phase indicates the presence of finite objects. On the basis of recent theoretical predictions [35], it has been shown that in correspondence to the isotropic to liquid crystalline columnar phase transition, columnar aggregates grow abruptly in length, but the growth can still proceed inside the liquid crystalline phase [12, 32]. Considering that, in the present case, the rod radii are roughly constant, the observed behaviour could be interpreted by supposing that the length of the rod-shaped aggregates increases inside the cholesteric phase. Therefore, in our system, a plausible picture would be finite columns, which grow slowly in length in the isotropic phase, lengthen abruptly when the isotropic to cholesteric phase transition is crossed and continue to grow in the cholesteric phase, so that, at the transition to the first 2-D phase, the rods are effectively infinitely long. Note that, according to the differences observed in the phase transition concentrations, in the case of the d(Gp)iBu derivative, the growth of aggregates in the isotropic phase could be slower. Such behaviour could be again associated with stereochemical constraints imposed by the presence of the isobutyl group, which could

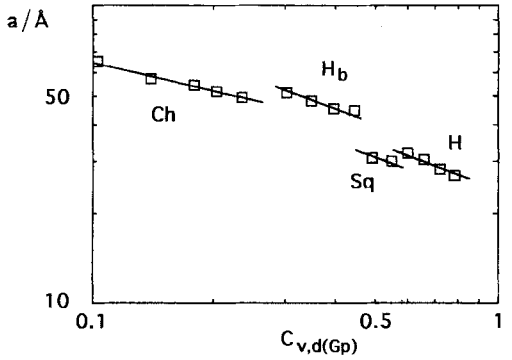


Figure 10. Variation of the unit cell dimension of the different phases observed for d(Gp) as a function of the d(Gp) volume concentration. A good fit for the cholesteric phase has been obtained with $a = 30{\cdot}7\ (C_{v,d(Gp)})^{-0{\cdot}33}$, while good fits for hexagonal, square and hexagonal $H_b$ phases have been obtained with $a = 23{\cdot}2\ (C_{v,d(Gp)})^{-0{\cdot}50}$, $a = 31{\cdot}3\ (C_{v,d(Gp)})^{-0{\cdot}50}$ and $a = 30{\cdot}1\ (C_{v,d(Gp)})^{-0{\cdot}50}$, respectively.

destabilize the stacking of the tetramers. It has been shown, in fact, that the structural characteristic of guanosine gels is the 4-stranded helix, where monomers grouped into tetramers stack helically. Interactions between adjacent disks are due to stacking forces and hydrogen bonds [4, 37]. It seems reasonable to assume that in the liquid crystalline phases too, hydrophobic interactions and hydrogen bonds may stabilize the columnar helicoidal aggregates. According to this, the esterification of the OH group in the 3′- or in 5′-position has different effects also on the stabilization of the columnar stacking: as previously observed, the d(pG) derivative exhibits hexagonal and cholesteric phases, while the isobutyl ester of d(pG) does not show any columnar lyomesophases [14].

### 3.7. *The columnar tetramer stacking*

The substitution of the H at $O_{3'}$ by the phosphate group or by the phosphate isobutyl ester group determines not only the occurrence of the described polymorphism, but also another structural peculiarity, not yet observed in other guanosine derivatives investigated. In fact, two observations seem to indicate that the guanosine residues which form the tetramers could assume a tilted arrangement inside the tetrameric plane. The first one concerns the magnetic behaviour of the cholesteric phase: as reported above, in this phase it was not possible to obtain the characteristic fingerprint or homogeneous planar textures, even after prolonged holding of samples in a magnetic field. It is evident that the possible tilt of the guanosine residues, which reduces the magnetic anisotropy, could explain such behaviour. The second observation is related to the values that the tetramer radius assumes in the Sq and $H_b$ phases. The tetramer radii, calculated considering that water does not penetrate the rods and with the assumption that the columns are infinite and have a circular section, appear to be smaller than the expected value of about 12·8 Å (observed in the hexagonal H phase and measured with molecular models [20]), and appear to decrease continuously as a function of the water content (see tables 2, 3, 4 and 5). It is evident that the reduction of the columnar cross section could be determined by an eventual tilted arrangement of the guanosine residues inside the tetrameric plane (note 2). Therefore, the observed variation of the tetramer radius appears to imply a continuous increase of such a tilt as the water content increases (see tables 3, 4 and 5). It should be emphasized that this arrangement does not require the tetrameric planes (i.e. the whole tetramers) to be tilted in the stacks: in fact, if this were so, the 3·4 Å tetramer stacking distance would have to be increased by a factor of $1/(\cos \alpha)$, where $\alpha$ is the tilt angle; the small error bars shown in figure 5 appear to rule this out.

The origin of the tilt could tentatively be interpreted considering that in the case of discotic molecules containing an aromatic core, the reduction of the hydrogen bond strength causes a stacking tilt [29]. In all the discotic systems investigated so far, we have considered that the force which holds together the tetramers in the columns derives from the balance between hydrophilic and hydrophobic interactions. It is evident that, by increasing the water content, changes in the hydration of the guanosine polar groups occur, determining a continuous reduction of the strength of the hydrogen bonds between adjacent tetramers. As a consequence, the hydrophobic interactions gain more and more importance in stabilizing the columnar stacking. In the present derivatives, the substitution of H at $O_{3'}$ imposes a series of steric constraints, so that in order to maximize the tetramer hydrophobic overlapping, the guanosine residues should tilt. Considering the phase diagram, such an arrangement could occur not only in the cholesteric, but also in the more ordered hexagonal $H_b$ and square Sq phases. It is noticeable that as a function of concentration, and also when phase boundaries are

crossed, the high angle X-ray diffraction peak shows the same position and width, indicating that the tetramer repeat distance and the stacking ordering remain quite constant. Therefore, even if the variation of stacking interactions could determine an unusual arrangement of the guanosine residues, the tetrameric planes appear not to be tilted in the stacks (note 3).

## 4. Conclusions

The peculiarity of the structural behaviour exhibited by d(Gp) and d(Gp)iBu has been demonstrated. In fact, even if the common structural unit of all the guanosine derivatives studied so far is the same (i.e. a chiral columnar aggregate composed of a stacking of Hoogsteen-bonded guanosine tetramers), both d(Gp) and d(Gp)iBu compounds exhibit a unique columnar polymorphism as well as an unusual $H_b$ hexagonal phase. The esterification of the H at $O_{3'}$ has particular effects on stabilization of both the columnar packing and the tetramer stacking. On the basis of the observed structural characteristics, we infer that the phase sequence is mainly determined by the occurrence of strong short-range intercolumnar interactions, while the steric encumbrance due to the presence of the phosphate or the phosphate isobutyl ester substituents seems to determine a tilted arrangement of the guanosine residues inside the tetrameric plane.

As a final conclusion, it could be underlined that the square and the $H_b$ hexagonal phases are new packing arrangements of molecular stacks that extend the range of chromonic phases structures.



We thank Dr S. Bonazzi for technical assistance. P. M. thanks Dr H. Franz for useful discussions and for a critical reading of the manuscript. The referees are also acknowledged for detailed comments and suggestions. This work was partially financed by MURST and CNR (Italy).

## Notes

(1) Considering the tetramer structure reported in figure 1, one might expect a slight depression in the electron density distribution at the centre of the tetrameric ring. However, in the three different phases, the central region of the rod section shows a maximum in electron density (see figure 8): this fact, which is, however, compatible with the presence of a large amount of ammonium ions inside the central hole, could also be related to the relatively low experimental resolution.

(2) The calculation of the tetramer radius could be discussed in more detail, because it is possible that the columnar aggregates are *finite in length.* In particular, if the length of the rods packed in the square Sq (p4, pos. (*a*)) and hexagonal $H_b$ (p6m, pos. (*b*)) lattices [21] is free to vary continuously, a 12·8 Å constant radius could also be calculated for these phases. Following this model, an estimation of the length of the columnar aggregates is given by the $L/C$ value, $L$ being the length of the rods and $C$ the repeat distance in the direction of $L$ [12, 32]. The $L/C$ value is observed to vary continuously from 0·97 (in the square phase) to 0·66 (in the hexagonal $H_b$ phase), indicating that the aggregate length increases as a function of concentration. However, in the present case, models based on the packing of finite aggregates present several problems: most significantly, as discussed above, the functional behaviour of the $a$ versus $C_{v,G}$ curves, which seems to indicate that the growth in length of the columns is accomplished in the isotropic and cholesteric phases. Furthermore, there is the absence of any detectable scattering (almost diffuse) corresponding to the length of the aggregates in the low angle diffraction region.

(3) This explanation is also supported by the behaviour of the structural parameter observed when the temperature changes. For example, in the case of d(Gp)iBu at $c = 0{\cdot}63$, the unit cell parameter relative to the square phase changes from 31·0 Å (at 5°C) to 30·2 Å (at 60°C), which corresponds to a decrease in the radius of the rod cross section from 12·6 Å to 12·3 Å. The strength of the hydrogen bonds is reduced when the temperature increases. As a consequence, the predominance of hydrophobic interactions between the stacked tetramers could then favour a tilted arrangement of the guanosine residues inside the tetrameric plane.

## References


[1] GELLERT, M., LIPSETT, M. N., and DAVIS, D. R., 1962, *Proc. natn. Acad. Sci. U.S.A.*, **48,** 2013.
[2] ARNOTT, S., CHANDRASEKARAN, R., and MARTTILA, C. M., 1974, *Biochem. J.*, **141,** 537.
[3] ZIMMERMAN, S. B., 1976, *J. molec. Biol.*, **106,** 663.
[4] SAENGER, W., 1984, *Principles of Nucleic Acid Structure* (Springer-Verlag), p. 315.
[5] SUNDQUIST, W. I., and KLUG, A., 1989, *Nature, Lond.*, **342,** 825.
[6] SEN, D., and GILBERT, W., 1988, *Nature, Lond.*, **334,** 364.
[7] SEN, D., and GILBERT, W., 1991, *Curr. Opin. Struct. Biology*, **1,** 435.
[8] SEN, D., and GILBERT, W., 1992, *Biochemistry*, **31,** 65.
[9] DETELLIER, C., and LASLO, P., 1980, *J. Am. chem. Soc.*, **102,** 1135.
[10] SPADA, G. P., CARCURO, A., COLONNA, F. P., GARBESI, A., and GOTTARELLI, G., 1988, *Liq. Crystals*, **3,** 651.
[11] MARIANI, P., MAZABARD, C., GARBESI, A., and SPADA, G. P., 1989, *J. Am. chem. Soc.*, **111,** 6369.
[12] AMARAL, L. Q., ITRI, R., MARIANI, P., and MICHELETTO, R., 1992, *Liq. Crystals*, **12,** 913.
[13] HOOGSTEEN, K., 1959, *Acta crystallogr.*, **12,** 822.
[14] BONASSI, S., CAPOBIANCO, M., DE MORAIS, M. M., GARBESI, A., GOTTARELLI, G., MARIANI, P., PONZI BOSSI, M. G., SPADA, G. P., and TONDELLI, L., 1991, *J. Am. chem. Soc.*, **113,** 5809.
[15] CARSUGHI, F., CERETTI, M., and MARIANI, P., 1992, *Eur. Biophys. J.*, **21,** 155.
[16] BONAZZI, S., DE MORAIS, M. M., GARBESI, A., GOTTARELLI, G., MARIANI, P., and SPADA, G. P., 1991, *Liq. Crystals*, **10,** 495.
[17] BONAZZI, S., DE MORAIS, M. M., GOTTARELLI, G., MARIANI, P., and SPADA, G. P., 1993, *Angew. Chem.*, **32,** 248.
[18] REESE, C. B., TITMAS, R. C., and YAU, L., 1978, *Tetrahedron Lett.*, 2727.
[19] TARDIEU, A., 1972, Ph. D. Thesis, Université Paris-Sud.
[20] FISK, C. L., BECKER, E. D., MILES, H. T., and PINNAVAIA, T. J., 1982, *J. Am. chem. Soc.*, **104,** 3307.
[21] *International Tables for X-Ray Crystallography*, 1952 (The Kynoch Press).
[22] LUZZATI, V., 1968, *Biological Membranes*, Vol. 1, edited by D. Chapman (Academic Press), p. 71.
[23] ATTWOOD, T. K., and LYDON, J. E., 1984, *Molec. Crystals liq. Crystals*, **108,** 349.
[24] LIVOLANT, F., and BOULIGAND, Y., 1986, *J. Phys., Paris*, **47,** 1813.
[25] SAEVA, F. D., 1979, *Liquid Crystals*, edited by F. D. Saeva (Marcel Dekker), p. 249.
[26] GOTTARELLI, G., PALMIERI, P., and SPADA, G. P., 1990, *Gazz. Chim. Ital.*, **120,** 101.
[27] SAKMANN, E., and VOSS, J., 1972, *J. chem. Phys. Lett.*, **14,** 528.
[28] DUDLEY, R., MASON, S. F., and PEACOCK, R. D., 1975, *J. chem. Soc. Faraday Trans.*, **2,** 997.
[29] WEBER, P., GUILLON, D., and SKOULIOS, A., 1991, *Liq. Crystals*, **9,** 369.
[30] IBALL, J., MORGAN, C. H., and WILSON, H. R., 1963, *Nature, Lond.*, **199,** 688.
[31] HARTSHORNE, N. H., and WOODWARD, G. D., 1973, *Molec. Crystals liq. Crystals*, **23,** 343.
[32] AMARAL, L. Q., GULIK, A., ITRI, R., and MARIANI, P., 1992, *Phys. Rev.* A, **46,** 3548.
[33] HENDRIKX, Y., and CHARVOLIN, J., 1992, *Liq. Crystals*, **11,** 677.
[34] CARTON, J. P., DUBOIS-VIOLETTE, E., and PROST, J., 1990, *Liq. Crystals*, **7,** 305.
[35] TAYLOR, M. D., and HERZFELD, J., 1991, *Phys. Rev.* A, **43,** 1892.
[36] HENTSCHKE, R., and HERZFELD, J., 1991, *Phys. Rev.* A, **44,** 1148.
[37] TOUGARD, P., CHANTOT, J. F., and GUSCHLBAUER, W., 1973, *Biochim. biophys. Acta*, **308,** 9.